Three Types of South Pacific Subtropical Mode Waters: Their Relation to the Large-Scale Circulation of the South Pacific Subtropical Gyre and Their Temporal Variability

doi: 10.1175/JPO3132.1

Three Types of South Pacific Subtropical Mode Waters: Their Relation to the Large-Scale Circulation of the South Pacific Subtropical Gyre and Their Temporal Variability

TAKAMASA TSUBOUCHI, TOSHIO SUGA, AND KIMIO HANAWA

Department of Geophysics, Tohoku University, Sendai, Japan

(Manuscript received 17 May 2006, in final form 18 December 2006)

ABSTRACT

A detailed spatial distribution of South Pacific Subtropical Mode Water (SPSTMW) and its temporal variation were investigated using the World Ocean Atlas (WOA) 2001 climatology and high-resolution expendable bathythermograph (HRX) line data. In the WOA 2001 climatology, SPSTMW can be classified into western and eastern parts. A detailed examination of spatial distributions using HRX-PX06 line data revealed that the eastern part can be further divided into two types by the Tasman Front (TF) extension. Consequently, SPSTMW can be classified into three types, referred to in the present study as the West, North, and South types. The West type, situated in the recirculation region of the East Australia Current (EAC), has a core layer temperature (CLT) of about 19.1°C; the North type, in the region north of the TF extension, has a CLT of about 17.6°C; and the South type, in the region south of the TF extension, has a CLT of about 16.0°C. The long-term (>6 yr) variations in the inventories of the three types were dissimilar to each other. The short-term (<6 yr) and long-term variations in the mean CLT of the North and South types were greater than that of the West type. Winter cooling in the previous year may have influenced the short-term variation in the South-type CLT. Moreover, the strength of the EAC may have influenced long-term variation in the West-type inventory and thickness and in the North-type thickness and CLT.

1. Introduction

Subtropical mode water (STMW), identified as a thermostad or a pycnostad, is formed in winter by intense vertical mixing. Because the evolution of the convection essentially depends on sea surface cooling, STMW is thought to memorize wintertime cooling at the sea surface. Additionally, the temporal variations in volume and temperature of STMW are considered to have an influence on upper ocean stratification and heat content because STMW has a relatively large volume in the subsurface ocean.

STMWs are reported to be located in the western part of the subtropical gyre in each ocean basin (Hanawa and Talley 2001). Because STMWs are formed under different conditions (e.g., the intensity of wintertime cooling and the strength of the associated western boundary current), their properties vary from one basin to another. STMWs located in the subtropical gyre in the Northern Hemisphere are formed under stronger winter cooling, are located in more intense recirculation regions of the western boundary currents, and appear to be more spatially homogeneous (Worthington 1959; Masuzawa 1969; Suga et al. 1997). In contrast, STMWs located in the subtropical gyre in the Southern Hemisphere generally are formed under weaker wintertime cooling and appear less spatially homogeneous (Gordon et al. 1987; Roemmich and Cornuelle 1992; Provost et al. 1999).

The factors influencing the basic features of STMWs such as degree of homogeneity, volume, temperature, and salinity are still not well understood. A comparison of STMWs in different ocean basins would be an effective way to understand the factors affecting their different features, because they are formed and distributed under different conditions (Roemmich and Cornuelle 1992). However, Southern Hemisphere STMWs have been much less studied than those in the Northern Hemisphere, partly because of limited data availability. As a result, formation areas and spreading paths of STMWs have not been described as clearly in the

Corresponding author address: Takamasa Tsubouchi, Department of Geophysics, Graduate School of Science, Tohoku University, Aoba-ku, Sendai 980-8578, Japan.
E-mail: t-taka@pol.geophys.tohoku.ac.jp

DOI: 10.1175/JPO3132.1

Southern Hemisphere as in the Northern Hemisphere. Therefore, studies of STMWs in the Southern Hemisphere would improve not only our knowledge of Southern Hemisphere STMWs themselves, but also our understanding of factors influencing the basic features of STMWs in the world's oceans.

The western South Pacific Ocean has been observed more than the western South Atlantic Ocean and the southwest Indian Ocean. For example, the annual number of temperature observations at depths of 200 m in the western South Pacific is greater than that in the western South Atlantic and the southwest Indian Ocean (Stephens et al. 2002). Consequently, the climatology in the World Ocean Atlas 2001 (WOA 2001; Stephens et al. 2002; Boyer et al. 2002) is more reliable for the western South Pacific than for the other basins of the Southern Hemisphere. A high-quality dataset from repeated high resolution expendable bathythermograph (HRX) lines crossing the distribution area of the South Pacific STMW (SPSTMW) is also available. Therefore, our research target for the present study is the SPSTMW.

SPSTMW was first described by Roemmich and Cornuelle (1992), who showed it to be a weak thermostad, with a temperature of 14°–20°C and a vertical temperature gradient less than 2.0°C $(100\ \text{m})^{-1}$, located in the western part of the South Pacific subtropical gyre. More recently, the inventory of SPSTMW observed in the PX06 line (see Fig. 2) has been shown to vary greatly over long time scales (Roemmich and Cornuelle 1992; Sprintall et al. 1995; Roemmich et al. 2005). However, the relationship between SPSTMW and the large-scale circulation of the South Pacific subtropical gyre, as well as the factors causing the temporal variations in its temperature, remains unclear.

The spatial structure of the large-scale circulation of the South Pacific subtropical gyre is considerably different from that of the North Pacific subtropical gyre. In this study, we refer to the large-scale circulation of the subtropical gyre as the current system including the western boundary current, the associated recirculation region, and the continuous eastward currents from the western boundary current. In the North Pacific subtropical gyre, the Kuroshio branches into the Kuroshio Extension and the Kuroshio Bifurcation. The main portion of the North Pacific STMW (NPSTMW) is located in the recirculation region of the Kuroshio and equatorward of the Kuroshio Extension (Hanawa 1987; Suga and Hanawa 1990, 1995; Oka and Suga 2003). In the large-scale circulation of the South Pacific subtropical gyre, the associated recirculation region of the East Australian Current (EAC) is much smaller, and the EAC separates into a series of filament-like eastward flows in the Tasman Sea (Ridgway and Dunn 2003; Roemmich et al. 2005).

In this study, we examined the detailed spatial distribution of SPSTMW and its relation to the large-scale circulation of the South Pacific subtropical gyre. Based on its spatial distribution and water properties, we classified SPSTMW into three types. We illustrate and examine possible factors causing the temporal variation in the inventories, thicknesses, and temperatures of these three water types on different time scales.

The contents of this paper are as follows. Section 2 describes the data and methods used in this study. The spatial distribution and classification of SPSTMW are described in section 3. In section 4, their temporal variations are examined and possible factors causing the temporal variation are discussed. Section 5 provides a summary and discussion.

2. Data and methods

SPSTMW is characterized by considerable seasonal variation and almost disappears in late autumn (Roemmich and Cornuelle 1992). In this study, we focused on the spatial distribution and temporal variation in SPSTMW observed in summer because SPSTMW is defined as a clear thermostad beneath the summer seasonal thermocline.

We used temperature and salinity data from the WOA 2001 and two HRX lines—the PX06 line running between Suva, Fiji, and Auckland, New Zealand, and the PX30 line running between Suva and Brisbane, Australia. The WOA 2001 climatology database is based on a $0.25° \times 0.25°$ (latitude $\times$ longitude) spatial grid at standard levels (0, 10, 20, 30, 50, 75, 100, 125, 150, 200, 250, 300, 400, 500, 600 m . . .). Temperature data were used to illustrate the spatial distribution of SPSTMW, and temperature and salinity data were used to calculate dynamic height relative to 1000 dbar.

The HRX data were obtained from the Scripps Institution of Oceanography Web site (http://www-hrx.ucsd.edu/index.html). The profiles were 30–40 km apart in midtrack and 10–20 km apart near the coast and over topographic features. Temperature data were usually available from the sea surface to 850-m depths in 2-m vertical bins, on average. The PX06 line was occupied 4 times a year from 1986 to 2003, including 29 transects from December to April. The PX30 line was also occupied four times a year from 1992 to 2005, including 24 transects from December to April. The HRX line data that we analyzed were from a different period (December–April) than the WOA 2001 climatology data (January–March), because in several years the PX30 line was not occupied from January to March. Prelimi-

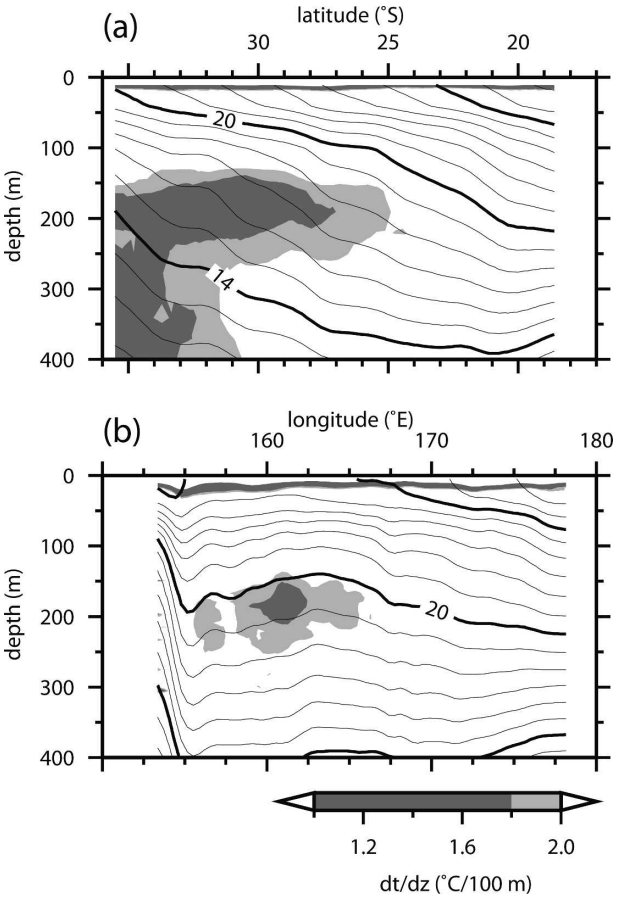

FIG. 1. Summer (December–April) average temperature section of (a) the PX06 line using 29 transects during 1986–2004 and (b) the PX30 line using 24 transects during 1992–2005. Shading shows the vertical temperature gradient [°C (100 m)$^{-1}$].

nary analysis indicated that the mean seasonal change in SPSTMW characteristics along the HRX lines during December–April is rather small, suggesting that this extended period can be used to represent the characteristics of SPSTMW in summer.

SPSTMW is defined as a water mass with a temperature of 14°–22°C and a vertical temperature gradient minimum less than 2°C (100 m)$^{-1}$ north of 30°S and less than 1.8°C (100 m)$^{-1}$ south of 30°S. We changed the definition of SPSTMW from that of Roemmich and Cornuelle [1992; a temperature range of 14°–20°C and a vertical temperature gradient minimum less than 2°C (100 m)$^{-1}$] to define SPSTMW as a thermostad with a minimum vertical temperature gradient. We implemented a stricter vertical temperature gradient criterion south of 30°S because the background temperature stratification of the study region weakens toward the south (Fig. 1a). It is difficult to detect a vertical temperature gradient minimum with the criterion of 2.0°C (100 m)$^{-1}$ south of 30°S. In addition, we extended the temperature range of the SPSTMW, because temperatures above 20°C are sometimes observed along the PX30 line. Even in the averaged section, SPSTMW along the PX30 line slightly exceeded the 20°C isotherm (Fig. 1b).

The core layer temperature (CLT) of SPSTMW is defined as the temperature at the absolute minimum of the vertical temperature gradient in SPSTMW for each profile and is expected to be the best record of the wintertime mixed layer condition.

The vertical temperature gradient of the WOA 2001 climatology and the HRX line data were calculated as follows. Our intention was to ensure that HRX line data had the same vertical resolution as WOA climatology data and to preserve a high horizontal resolution. The standard depth grid of the WOA 2001 climatology data was interpolated to 10-m vertical intervals using Akima's shape-preserving local spline (Akima 1970). The vertical temperature gradient at a given depth was calculated based on the difference between temperatures 10 m above and below. The HRX line data were first smoothed vertically using a 3-point (window of 6 m) median filter 30 times to smooth out vertical temperature structure smaller than about 60 m. The data were then gridded horizontally at 40-km intervals using a Gaussian filter with an *e*-folding scale of 60 km. This filtering smoothed out disturbances with horizontal length scales smaller than about 200 km, while resolving temperature fronts running across HRX lines. The vertical temperature gradient at a given depth was calculated using temperatures 2 m above and below.

Monthly wind stress data and heat flux data from the 40-yr European Centre for Medium-Range Weather Forecasts (ECMWF) reanalysis (ERA-40; Simmons and Gibson 2000) were used. The data period was from 1957 to 2002, and the spatial grid scale was 2.5° × 2.5°. Monthly mean sea surface temperature (SST) data prepared by Reynolds et al. (2002) were also used, with a data period from 1971 to 2000 and an original spatial grid scale of 2° × 2°. The SST data were resampled onto the 2.5° × 2.5° ECMWF grid using a Gaussian filter with an *e*-folding scale of 500 km.

3. Spatial structure of SPSTMW

a. Relationship between SPSTMW and the large-scale circulation in the WOA 2001 climatology

Our purpose in this section is to describe in detail, using the WOA 2001 climatology, the spatial distribution of SPSTMW and its relation to the large-scale circulation of the South Pacific subtropical gyre. Figure 2

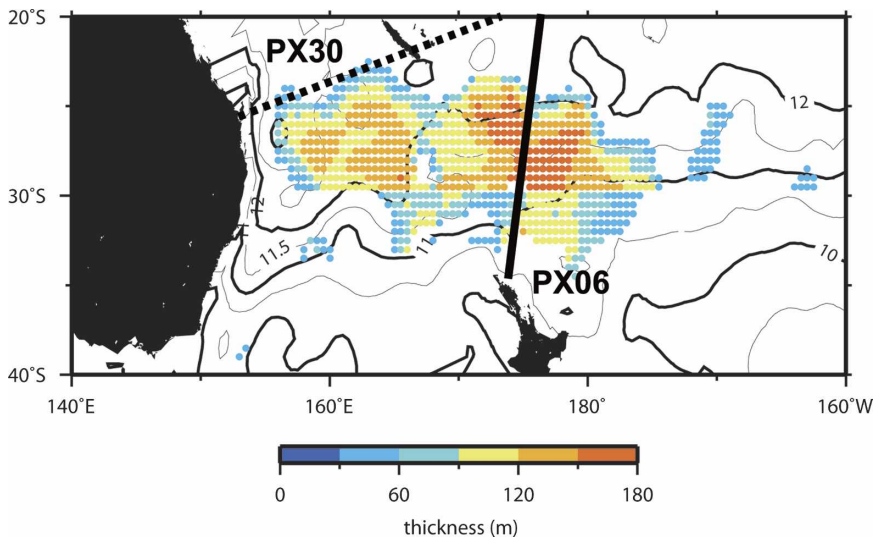

FIG. 2. Spatial structure of the thickness (m) of SPSTMW and the mean position of the HRX lines. The PX06 line (solid line) and the PX30 line (dotted line) are superimposed on the dynamic height ($m^2\ s^{-1}$) at 180 dbar relative to 1000 dbar, calculated using WOA 2001 climatology.

shows the spatial distribution of SPSTMW thickness superimposed on the dynamic height at 180 dbar. This depth was chosen because the core layers of SPSTMW are generally observed around 180 dbar. Although the thickness of SPSTMW appeared to change abruptly across 30°S, this change was the result of the changing definition of SPSTMW. Two separate thickness maxima are situated around 160° and 175°E in the 25°–30°S latitudinal band. Although these separate thickness maxima are marginally distinguished in the map of Roemmich and Cornuelle (1992, their Fig. 2c), they did not mention this feature. The maximum around 160°E was located in the recirculation region of the EAC and the adjacent area of weak flow on the equatorside of the dynamic height of the 12.0 $m^2\ s^{-2}$ contour. In contrast, the maximum around 175°E was located in the region of broad eastward flow.

Core layer water properties of major portions of each part were analyzed to further examine properties of the two SPSTMW thickness maxima. Here, the major portion was defined as the area of the SPSTMW layer with a thickness greater than 120 m north of 30°S and 60 m south of 30°S (Fig. 3a). The criteria of 120 and 60 m were selected to spatially separate the two thickness maxima. The resulting temperature–salinity (θ–S) diagram shows that the water properties of these two maxima differed (Fig. 3b). The water properties of the western maximum were fairly uniform and centered on about 19.0°C and 35.65 psu. In contrast, the eastern maximum showed a much wider range of temperature and salinity, 15.0°–18.5°C and 35.35–35.65 psu. The CLT of the western and eastern thickness maxima formed a mode class around 19.0° and 17.0°C, respectively (Fig. 3c). It is also notable that Norfolk Ridge is situated between the western and eastern maxima, and this topographic feature may affect upper ocean temperature structure, especially on the Tasman Front (TF; Stanton 1979; Mulhearn 1987; Tilburg et al. 2001).

Here we classified SPSTMW into two parts based on the spatial distribution of its thickness and water properties. The western part, defined as a thermostad located in the region west of 167°E and north of 30°S, was situated within the recirculation region of the EAC and had fairly uniform water properties. The eastern part, defined as a thermostad located in the region east of 167°E or south of 30°S, was situated within the broad eastward flow and had a wider range of temperature and salinity.

b. *Relationship between the eastern part of SPSTMW and temperature fronts in the PX06 line section*

The large-scale circulation depicted in the WOA 2001 climatology (Fig. 2) differed somewhat from previous descriptions. Although WOA 2001 climatology shows the broad eastward flow as a continuous extension of the EAC, it has been reported that EAC outflow from the western boundary splits into a series of eastward and northeastward currents (Ridgway and Dunn 2003, their Fig. 7). The WOA 2001 climatology does not show the filaments of the eastward flow because its temporally and spatially smoothed field can-

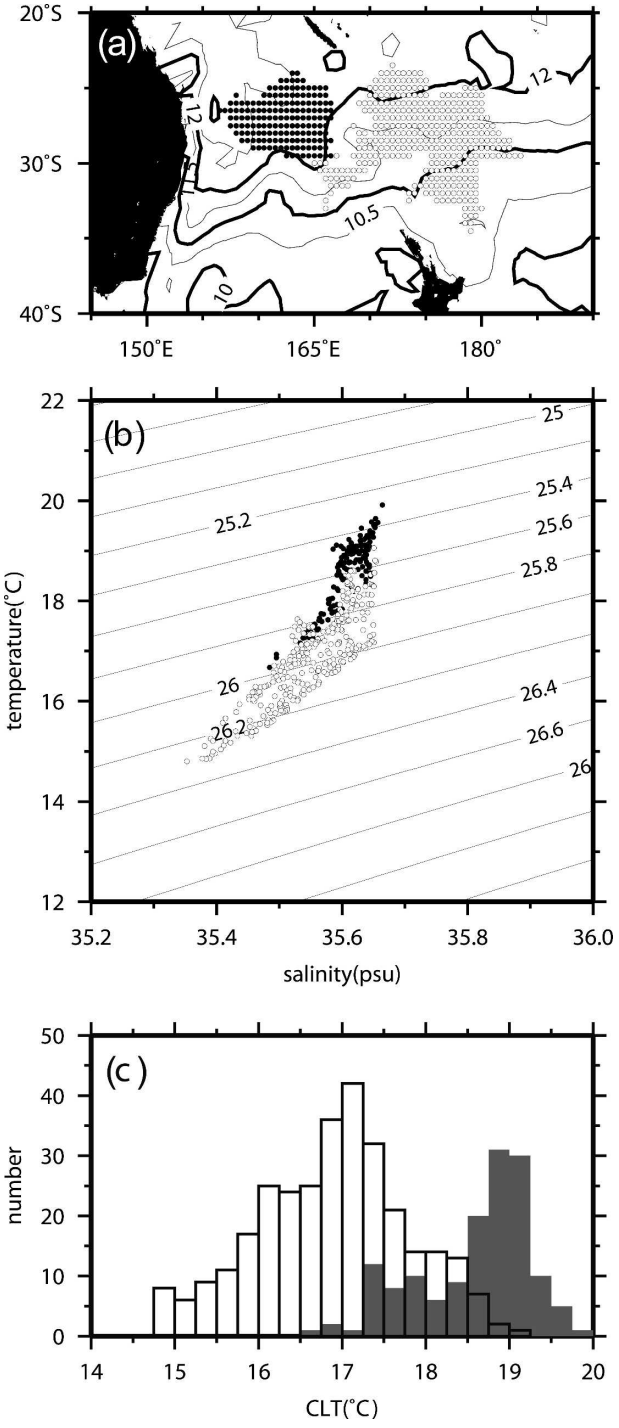

FIG. 3. (a) Spatial distribution, (b) θ–S diagram, and (c) histogram of CLT having sufficient thickness. Water properties west of 167°E and north of 30°S with a thickness greater than 120 m are plotted as closed circles in (a) and (b) and as gray bars in (c). Water properties east of 167°E and with a thickness greater than 120 m or those south of 30°S with a thickness greater than 60 m are plotted as open circles in (a) and (b) and as open bars in (c). The contours of (a) show the dynamic height ($m^2\ s^{-1}$) at 180 dbar, as in Fig. 1.

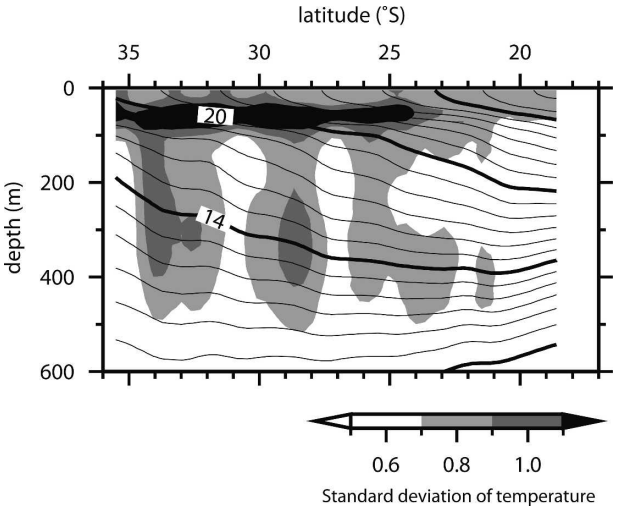

FIG. 4. Mean temperature (°C; contours) and std dev of temperature (shading) for the PX06 line section calculated from 29 summer (December–April) transects during 1986–2004.

not preserve fine flow patterns. Because the eastern part of SPSTMW is situated in the region of these filament currents, the WOA 2001 climatology presumably does not fully resolve the spatial distribution of the eastern SPSTMW.

The PX06 line crosses the eastern part of SPSTMW and the region with the eastward flow filaments extending from the EAC (Fig. 2). A temperature front associated with the East Auckland Current (EAUC) is shown to be located north of New Zealand, and the continuation of the TF runs along about 29°S in the PX06 line section (Roemmich and Cornuelle 1990). We detected temperature fronts in the PX06 line section in summer and describe the relationships between the fronts and SPSTMW.

Figure 4 shows the mean temperature section averaged over all 29 summer transects from 1986 to 2004 and the associated standard deviations. This section of the standard deviations almost resembles that of Roemmich and Cornuelle (1990, their Fig. 5), who calculated standard deviations using all transects irrespective of season from 1986 to 1990. The main difference between their result and ours is seen in the layers from the sea surface to a depth of 50 m. The standard deviations at 0–50-m depth in our section were much smaller because of the exclusion of seasonal cycles. Otherwise the two sections had almost the same characteristics. As Roemmich and Cornuelle (1990) mentioned, the maximum standard deviations around 34°, 29°, and 23°S of around 250–500 m corresponded to the EAUC, the continuation of the TF, and the Tropical Convergence, respectively.

We also examined the maximum of 21°–27°S around

80–180 m, which also marginally appeared in Roemmich and Cornuelle (1990) but was not discussed. We carefully examined the 21°–27°S latitudinal band and subjectively found that one or two temperature fronts appeared in this region in each section: one temperature front appeared in 18 sections and two fronts appeared in 11 sections out of 29 summer sections during 1986–2004. In addition, a temperature front always appeared between 21° and 24.5°S and only occasionally between 24.5° and 27°S. These fronts should correspond to the filaments of eastward flow extending from the EAC (Ridgway and Dunn 2003). In this study, we regarded the temperature front situated in the 21°–24.5°S latitudinal band as a permanent front. Consequently, we detected three temperature fronts. We regarded the temperature fronts around 34°, 29°, and 21°–24.5°S as those associated with the EAUC, the continuation of the TF, and the signature of an eastward current, respectively.

Although much research has examined the TF (Stanton 1979; Mulhearn 1987), it has not been clearly defined. The TF is reported to become weaker after passing the Lord Howe Rise (Stanton 1979; Mulhearn 1987; Ridgway and Dunn 2003), but few studies have monitored the TF after it passes this point. Therefore, the positions of three temperature fronts in each section were defined as those where the horizontal temperature gradient averaged over 100–500-m depths had a maximum south of 32°S and around 27°–31°S, and that averaged over 100–200-m depths had a maximum around 21°–24.5°S. The three segments used to detect front positions corresponded to the areas with large standard deviations. Hereafter, we will refer to these three fronts around 34°, 29°, and 23°S as the EAUC front, the TF extension, and the 23°S front, respectively.

We examined the relationship between the above defined temperature fronts and SPSTMW in the PX06 line section starting with an inspection of individual sections (e.g., April 1988). In this section, SPSTMW was clearly divided by the TF extension (Fig. 5a). The 23°S (EAUC) front was located on the northern (southern) edge of SPSTMW. The CLT increased by 2.1°C northward across the TF extension and was meridionally uniform over 400–500 km on either side of the TF extension (Fig. 5b). The CLT distribution appeared to be characterized by two zones with distinct and fairly uniform CLT divided by the TF extension and bounded to the north (south) by the 23°S (EAUC) front. This structure was substantially different from that depicted in the WOA 2001 climatology, where the CLT of the eastern part of SPSTMW increased gradually to the north (not shown). The same situation as in the WOA

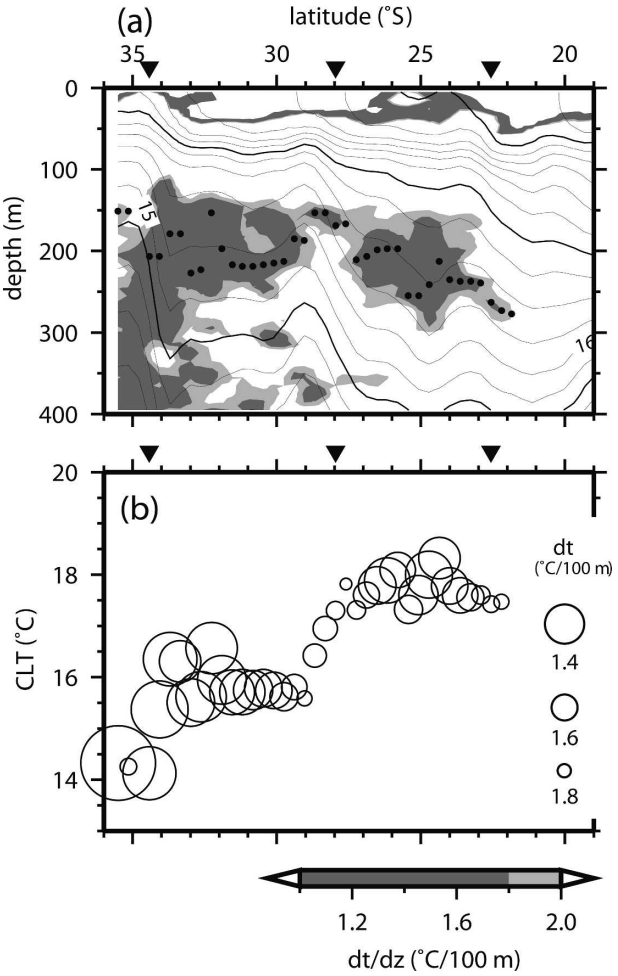

FIG. 5. (a) Temperature (°C) section in the PX06 line from April 1998. Shading shows the vertical temperature gradient [°C (100 m)$^{-1}$], and closed circles show the depth of the CLT. (b) Scatterplots of CLT vs latitude. The size of the circles represents the vertical temperature gradient. Triangles at the top of the panels show the positions of the EAUC front, the TF extension, and the 23°S front, respectively.

2001 climatology appeared in the average section of the PX06 line (i.e., no significant temperature front existed in the section; Fig. 1a). While the positions of the fronts and the absolute values of the CLT differed from one section to another, we found essentially the same relationship between SPSTMW and the fronts in the other individual sections. Mean temperature sections indicate that the 23°S (EAUC) front was located at the northern (southern) boundary of SPSTMW (Fig. 1a). The northern (southern) boundary of SPSTMW was almost 25°S (33°S), corresponding to the standard deviation maxima in the PX06 line section (Fig. 4).

To characterize the mean spatial structure of SPSTMW relative to the TF extension, we averaged the CLT over the entire summer period with respect to the meridi-

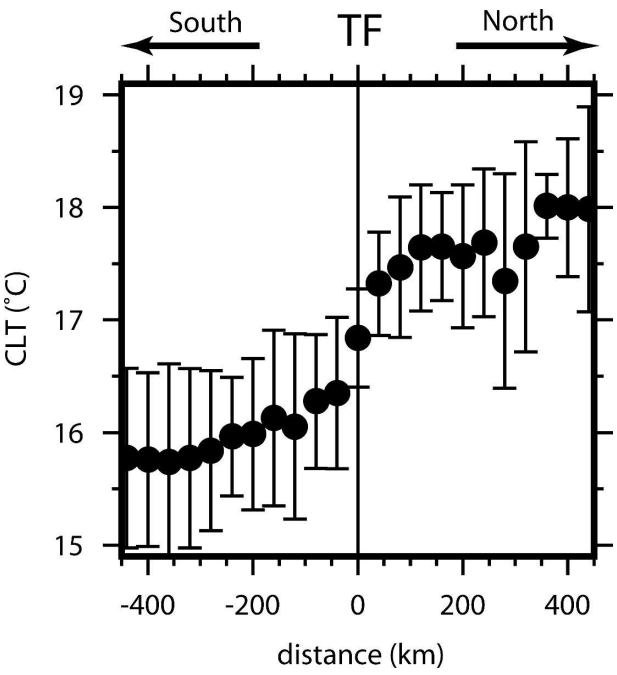

FIG. 6. Averaged CLT distribution using frontal coordinates with respect to TF extension in summer (December–April). Error bars show the std dev of CLTs using frontal coordinates with respect to the TF extension.

onal coordinate using the position of the TF extension as its origin (Fig. 6). Similar methods have been used to depict the mean hydrographic structure near the Kuroshio Front in the western North Pacific (Hanawa and Hoshino 1988; Bingham 1992). Figure 6 clearly demonstrates that the CLT increases to the north about 1.5°C across the TF extension but is relatively meridionally uniform over about 400 km to either side of the TF extension. This mean structure of CLT suggested that the eastern part of SPSTMW could be further classified into two types.

c. Three types of SPSTMW

The mean pictures of SPSTMW based on the WOA 2001 climatology and the PX06 line data are combined consistently as follows. SPSTMW in the WOA 2001 climatology was classified into western and eastern parts. Considering the spatial distribution of CLT in the PX06 line section, the eastern part of SPSTMW was further divided into two types. The key to this latter classification was the abrupt change of CLT across the TF extension in the PX06 line section. This abrupt change was only detected in individual sections or through the averaging procedure using a meridional coordinate with respect to the TF extension, because the TF extension position varies and the CLT north and south of the TF extension changes from year to year.

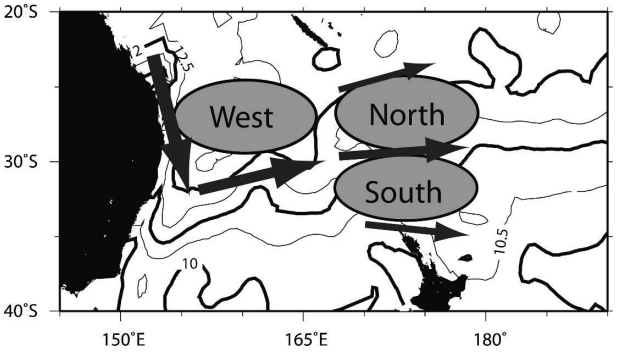

FIG. 7. Schematic synoptic spatial distribution of three types of SPSTMW and the large-scale circulation (arrows). The contours show the dynamic height ($m^2\ s^{-1}$) at 180 dbar, as in Fig. 1.

Therefore, we could not find the abrupt change in CLT in the WOA 2001 climatology. However, by combining the images based on the WOA 2001 climatology and the PX06 line data, the SPSTMW was classified into three types.

We propose a schematic synoptic spatial distribution of SPSTMW in the South Pacific subtropical gyre (Fig. 7). The SPSTMW consists of three types: the West, North, and South types. The West type is located in the recirculation region of EAC and has a CLT of about 19.1°C. The North type is located in the region between the 23°S front and the TF extension and has a CLT of about 17.6°C. The South type is located in the region between the TF extension and the EAUC front and has a CLT of about 16.0°C. The TF extension, EAUC front, and the 23°S front are not spatially fixed boundaries; rather, they shift over time. This spatial pattern and relation to a series of filament flows as continuous flows from EAC are quite different from that of NPSTMW, the North Pacific counterpart of SPSTMW.

4. Temporal variation in three types of SPSTMW and its possible causes

a. Temporal variation observed in the HRX lines

The PX06 line crosses the North and South types of SPSTMW meridionally and the PX30 line crosses the northern part of the West type almost zonally (see Fig. 2). Although the PX30 line is located at the northern margin of the West type in the climatological map (Fig. 2), the West type always appears in individual PX30 line sections. We defined the inventory, mean thickness, and mean CLT of each type in every summer section for the entire period to investigate the temporal variation in SPSTMW. The inventory was defined as the area observed in assigned segments of each section. The segments of the sections used to calculate inventory of the three types were a segment west of 167°E for

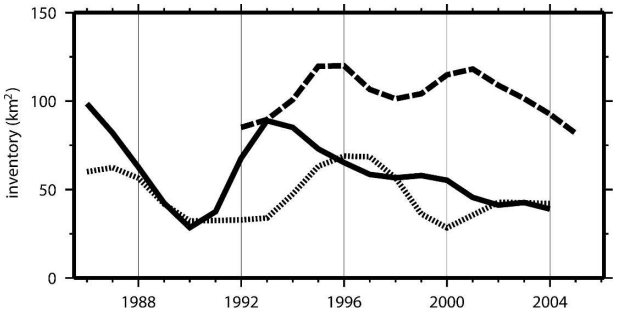

FIG. 8. Time series of long-term variation in inventory of the West, North, and South water types, shown as dashed, solid, and dotted lines, respectively.

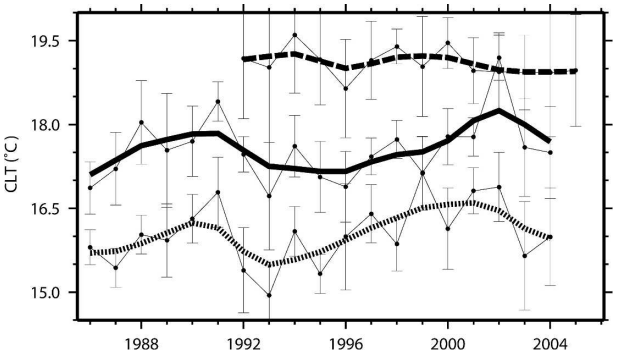

FIG. 9. Time series of CLT of the three water types. Thin and thick lines show the gridded time series and the long-term variation, respectively. Error bars show gridded value of the std dev in calculation of the mean CLT in each section. The West, North, and South types of SPSTMW are shown as dashed, solid, and dotted lines, respectively.

the West type, a segment between the TF extension and the 23°S front for the North type, and a segment between the TF extension and the EAUC front for the South type. The sectional mean CLT (thickness) of each of the three types was defined by averaging the CLT (thickness) in each assigned segment. The segments of the sections used to calculate the mean CLT and mean thickness of the three types were 155°–165°E for the West type and 50–450 km north (south) of the TF extension for the North (South) type.

The HRX line data include one to three repeat measurements per summer (December–April). To make the data gridded at 1-yr intervals, we filtered the time series of inventory, mean thickness, and mean CLT using a Gaussian filter with a 1-yr half-power point having a 0.5-yr filter window. This calculation effectively meant that if only one section was measured in a summer, these single values of inventory, mean thickness, and mean CLT were adopted as the values for the entire summer; if two or three sections were measured in a summer, the average values were adopted. These original gridded time series were low-pass filtered using a Gaussian filter with a 6-yr half-power point to evaluate long-term variation. Time series representing short-term variation were obtained by subtracting the low-pass-filtered time series from the original gridded time series. The long-term and short-term variation in the reanalysis flux data was also evaluated in the same manner.

The HRX line time series are somewhat short for investigating long-term variation. The criteria for measuring the significance of correlation coefficients of long-term variability were calculated using t-distribution checking. Degrees of freedom were calculated using the zero crossing autocorrelation scale of each time series. We used the 5% significance level to evaluate correlation coefficients.

Figure 8 shows the long-term temporal variation in the inventories of the three types. The inventories of the three types showed dissimilar temporal variation. The West type had maxima in 1995–96 and 2001 and a minimum in 1998. The North type had a minimum in 1990 and a maximum in 1993 and gradually decreased after that point. The South type had minima in 1990–93 and 2000 and maxima in 1995–97. These long-term variations were primarily determined by long-term variations in thickness rather than in meridional extent. Correlations between time series of thickness and of inventory of the three types were significantly positive with correlation coefficients of 0.96, 0.96, and 0.92 for the West, North, and South types, respectively. Although the meridional extent of each type varied to some degree, the correlations between time series of meridional extent and of the inventory of the three types were not significant. The large long-term variation in inventory observed in the PX06 line can reportedly be regarded as variation in the single water mass (Roemmich et al. 2005). Figure 8 shows that maxima in the North type in 1993 and the South type in 1995–97 together contributed to the prolonged maximum in 1992–96 reported by Roemmich et al. (2005).

Figure 9 shows the original gridded and low-pass-filtered CLT time series of the three types of SPSTMW. The North and South types had large long-term variation, while the West type had a small degree of variation. The standard deviations of long-term variation in the West, North, and South types were 0.12°, 0.33°, and 0.34°C, respectively. The North type had maxima in 1991 and 2002 and a minimum in 1993–96. The South type had maxima in 1990 and 2001 and a minimum in 1993. The short-term variations were larger in the North and South types than in the West type. The standard deviations of short-term variation in the West, North, and South types were 0.19°, 0.38°, and 0.39°C,

respectively. A significant negative correlation (−0.82) was found in the long-term variation of the North type between the inventory and CLT time series, indicating that the larger volume of the North type tends to have a colder CLT.

We will not discuss the short-term temporal variation in inventory in this study because there were only one–three sections per summer. While short-term variation in inventory is highly influenced by mesoscale eddies, that in CLT is not. Although a mesoscale eddy does not change the water mass temperature, it dynamically distorts the isotherm. That is, the extension (squeeze) of the isotherm interval by an anticyclonic (cyclonic) eddy makes the inventory of SPSTMW greatly increase (decrease). Thus, inventory should be sensitive to mesoscale eddies, unlike mean CLT. The time series of short-term inventory obtained from HRX line data were not appropriate for describing representative year-to-year variation in inventory. In contrast, the time series of long-term inventory obtained from HRX line data were appropriate for describing representative long-term variation in inventory because averaging the inventory over several years should cancel out the influence of mesoscale eddies.

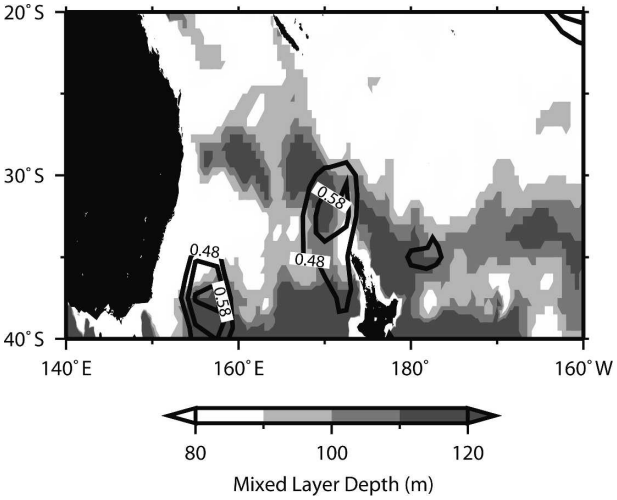

FIG. 10. Correlation coefficients exceeding the significance level of 5% between short-term variation of CLT of the South type and that of the heat flux at each grid point [positive (negative) significant correlation coefficients denoted by thick (dotted) line] superimposed on the mixed layer depth (shading; m) in winter. The mixed layer depth is defined as a depth where temperature is 0.5°C lower than the SST.

b. Factors causing temporal variation

In the North Pacific, short-term variation in the CLT of NPSTMW is shown to be influenced by the strength of wintertime cooling (Taneda et al. 2000), and the long-term variation in CLT is influenced by the strength of the Kuroshio transport (Hanawa and Kamada 2001). We examined the factors causing the temporal variation in SPSTMW, considering these previous results for NPSTMW. We examined winter cooling as a possible factor affecting short-term variation in CLT, and winter cooling and the strength of EAC as possible causes of long-term variation in inventory, thickness, and CLT.

The degree of winter cooling is defined as the summation of sea surface heat flux and the Ekman heat divergence and is hereafter referred to as heat flux. Because the monthly average heat flux for April–September is negative, we defined the degree of winter cooling in a given year as the average heat flux during this period. In contrast, defining the transport of a western boundary current is complicated because of the difficulty in determining the offshore edge of the western boundary current (Gilson and Roemmich 2002). Because appropriately defining the EAC transport is not an easy task, the strength of EAC for a given year was estimated by the wind forcing over the South Pacific subtropical gyre. It has been reported that the wind stress curl in the central North Pacific leads the Kuroshio transport by some years (Yasuda and Kitamura 2003; Wakata et al. 2006). As a proxy for the EAC transport, the annual mean streamfunction of the Sverdrup transport at 156.25°E and 28.75°S was defined. This will represent the Sverdrup transport corresponding to the EAC, because the streamfunction has a maximum at this point in the western South Pacific.

If winter cooling is the main factor causing short-term variation in CLT, an area where the heat flux variation is highly correlated with CLT variation will appear in a probable SPSTMW formation area. Additionally, the probable formation areas would be roughly identified as the areas of deep mixed layers upstream of each of the three types in the HRX lines. We calculated a correlation coefficient between short-term variation in the mean CLT for each of the three types and that of heat flux. Figure 10 shows where the correlation coefficient between the short-term variation in CLT of the South type and that of heat flux at each grid point exceeded the significance level of 5%. A significant positive correlation appeared around 167°–172°E, 29°–38°S. This area contains the deep winter mixed layer, which is evaluated by the mixed layer depth calculated from the WOA 2001 winter (July–September) climatology as the depth where the temperature is 0.5°C lower than SST. Also, the 29°–34°S latitudinal band corresponds to upstream of the South type in the PX06 line. No significant correlation was found between the short-term variation in CLT of the West

and North types and heat flux in the probable formation areas.

The area of positive significant correlation coinciding with deep mixed layers in the probable formation area suggests that short-term variation in CLT of the South type was mainly influenced by winter cooling. The positive correlation suggests that stronger (weaker) winter cooling causes colder (warmer) CLT. We cannot exactly determine the formation area of the South type in the present analysis. This research topic would require further analysis and is beyond the scope of this study. The lack of significant correlation for the West type may be due to the low signal-to-noise ratio because the West type has small short-term variation in CLT. The lack of significant correlation for the North type may be the result of the small absolute value of inventory, indicating that the CLT of the North type is difficult to properly detect in some years, especially during 1988–92 and 2001–03. Note that the South type has a stricter vertical temperature gradient. Although the averaged inventory of the South type for the entire period was comparable to that of the North type (Fig. 8), the South type was actually a more homogeneous thermostad. Thus we expect that the South type better conserves the winter mixed layer conditions.

We examined the correlation between long-term variation in CLT and heat flux and between long-term variation in inventory and heat flux. No significant correlation was found between long-term variation in the CLT of all types and heat flux in the probable formation area. Similarly, no significant correlation was detected between long-term variation in inventory of all types and that of heat flux in probable formation areas. While the analyzed time series may be short, our results imply that heat flux did not have a significant influence on the long-term variation in all types of SPSTMW.

Lag correlation analyses between long-term variation in inventory, thickness, and CLT and that of the Sverdrup transport representing the EAC transport were also performed. The inventory and thickness of the West type had significant negative correlations (-0.90 and -0.92) with the lag of 12 yr. The thickness of the North type was significantly negatively correlated -0.81) with the lag of 10 yr, and its CLT had a significant positive correlation (0.82) with the lag of 9 yr. Here lag correlation analysis was not applied to the CLT of the West type, which did not show large long-term variation. The lag correlation analysis results are summarized in Table 1.

The lag between the Sverdrup transport and the EAC transport can be roughly estimated as follows. The first baroclinic mode of a westward-moving Rossby wave is regarded as a main information carrier of the up-and-down movement of the thermocline, which will eventually change the EAC transport. The change in EAC transport will lead the advection downstream to the formation zone, and thus affects the formation rate. Maharaj et al. (2005) estimated the phase speed of the long Rossby wave in the South Pacific using satellite observation data. Based on their results, we roughly estimated the propagation time of the first mode Rossby wave from the central South Pacific to the eastern coast of Australia at 30°S as 5–8 yr. This value is a shorter time than the lag of 9–12 yr calculated by the present analysis. The difference may result from the influence of irregularity in western South Pacific bottom topography. This topography may excite higher Rossby wave modes with lower propagation speeds, which also play a role in the westward propagation of the thermocline movement.

TABLE 1. Summary of the results of the lag correlation analysis between the long-term variation in thickness, inventory, and CLT of the three types of SPSTMW and that of Sverdrup transport. The number of years in parentheses denotes the lag, i.e., the Sverdrup transport leads.

	West type	North type	South type
Thickness	−0.92 (12 yr)	−0.81 (10 yr)	Not significant
Inventory	−0.90 (12 yr)	Not significant	Not significant
CLT	—	0.82 (9 yr)	Not significant

The above estimation of Rossby wave propagation time implies the tendency that when EAC is strong (weak), less (more) and warmer (colder) SPSTMW will be formed. We interpret this result as follows. When the EAC becomes stronger (weaker), warmer (colder) water is supplied to the SPSTMW formation area. This makes the water column of the formation area warmer (colder). At the same time, a stronger EAC will possibly make the stratification in the formation area more intense because the advective warming is larger in the upper ocean because of the higher velocity and along-flow temperature gradient in the shallow layer. Thus the stronger EAC carries more upstream warmer water to the formation area and possibly makes stratification in the formation area more intense. As a result, with the delay of 9–12 yr after the enhanced Sverdrup transport, the inventory and thickness of the West and thickness of the North type decreases, and CLT of the North type increases.

5. Summary and discussion

The purpose of this study was twofold. First, we examined the detailed spatial distribution of SPSTMW and classified SPSTMW into three types, taking into

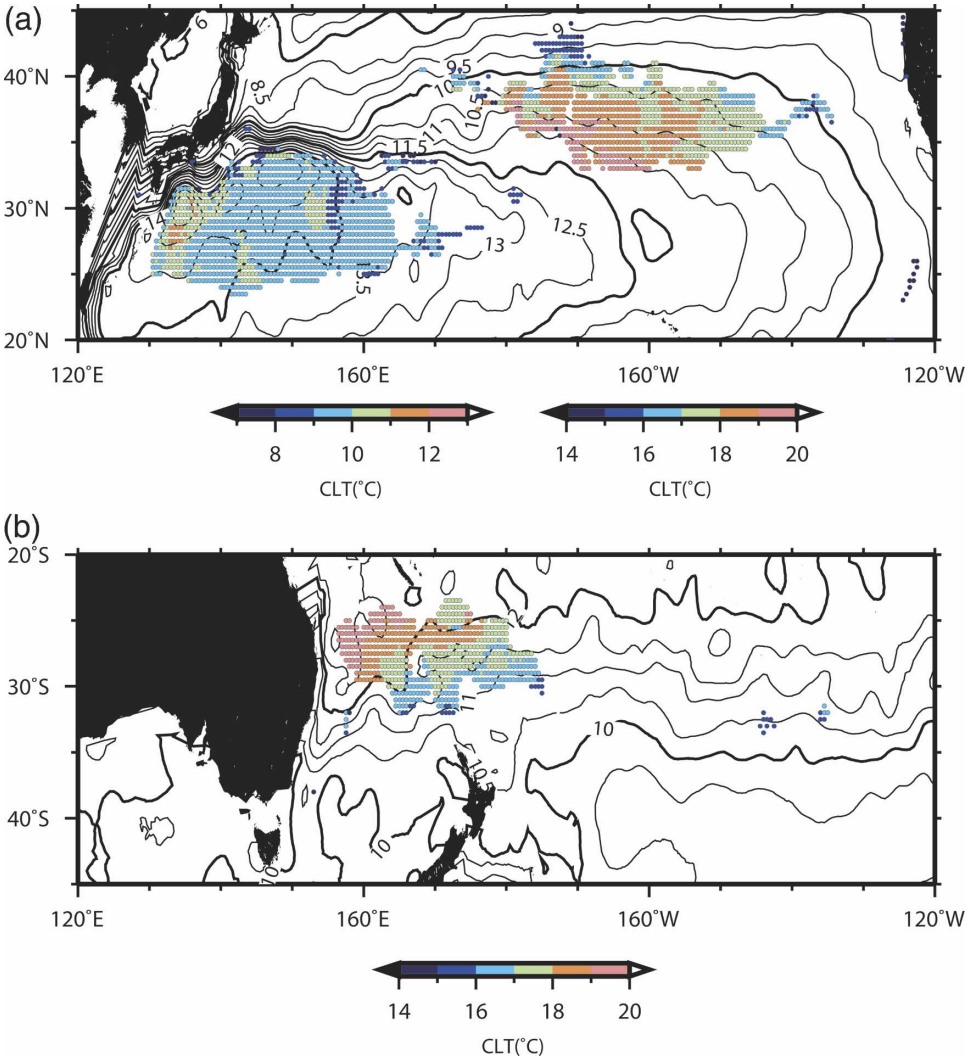

FIG. 11. (a) Distribution of CLT of the thermostad in the North Pacific with a thickness greater than 80 m, temperature of 14°–20°C, and vertical temperature gradient less than 2.0°C (100 m)$^{-1}$ (right color scale); or that with a temperature of 7°–13°C and vertical temperature gradient less than 1.6°C (100 m)$^{-1}$ (left color scale). (b) Distribution of CLT of the thermostad in the South Pacific with a thickness greater than 80 m, a temperature of 14°–20°C, and a vertical temperature gradient less than 2.0°C (100 m)$^{-1}$. Contours showing the dynamic height (m^2 s^{-1}) at 180 dbar are superimposed.

account several features of SPSTMW detected in the WOA 2001 climatology and the PX06 line section: the spatial distribution, water properties, and relation to the large-scale circulation, including variable filament currents. Based on the WOA 2001 climatology, we first classified SPSTMW into two parts, the western and eastern parts. Based on the PX06 line data, which cross the eastern part meridionally, we showed that the eastern part is further divided into two types by the TF extension. The CLT changes by about 1.5°C across the TF extension in the mean section constructed using a meridional coordinate with respect to the TF extension. Accordingly, we concluded that SPSTMW is classified into three types: the West, North, and South types (Fig. 7). The West type is located in the recirculation region of EAC and has a CLT of about 19.1°C. The North type is located in the region between the 23°S front and the TF extension and has a CLT of about 17.6°C. The South type is located in the region between the TF extension and the EAUC front and has a CLT of about 16.0°C.

The second part of this study described the temporal variation in the three types of SPSTMW using HRX line data and examined possible factors causing the temporal variation on different time scales. The three types differed in the long-term variation in inventory.

The short-term and long-term variations in mean CLT of the North and South types were large, while that of the West type was small. We examined the heat flux and EAC transport represented by the Sverdrup transport as factors influencing temporal variation. Short-term variation in heat flux may influence the short-term variation in CLT of the South type, and long-term variation in the strength of the EAC may possibly influence the long-term variation in inventory and thickness of the West type and the long-term variation in thickness and CLT of the North type.

The results of this study will help advance our general understanding of STMW through an intercomparison among STMWs in different basins. Here we briefly compare SPSTMW with NPSTMW and North Pacific Central Mode Water (NPCMW). Figure 11 shows the spatial distribution of the CLT of thermostads with a thickness greater than 80 m superimposed on the dynamic height at 180 dbar in the North Pacific and South Pacific. A thermostad with a temperature of 14°–20°C is defined as a layer with a vertical temperature gradient less than 2.0°C $(100\ \text{m})^{-1}$, and a thermostad with a temperature of 7°–13°C is defined as a layer with a vertical temperature gradient less than 1.6°C $(100\ \text{m})^{-1}$. According to previous studies, the thermostads around 130°–165°E and around 180°–145°W in the North Pacific correspond to NPSTMW (Masuzawa 1969; Suga and Hanawa 1995) and NPCMW (Nakamura 1996; Suga et al. 1997), respectively. SPSTMW is identified as the thermostad around 155°E–175°W in the South Pacific.

NPSTMW is located in the large recirculation region of the Kuroshio and has a nearly uniform CLT of 16°–17°C, whereas SPSTMW is located in the small recirculation region of EAC (the West type) and a region of weak eastward flow (the North and South types) and has a larger CLT range of 14°–20°C. As far as the relation between narrow CLT range and the tight relation to recirculation are concerned, the West type of SPSTMW appears to correspond to NPSTMW. In contrast, the North and South types resemble NPCMW with its wide CLT ranges and distributions in the eastward flow. Furthermore, using repeat hydrographic section data, Oka and Suga (2005) showed that NPCMW is classified into two types divided by the Kuroshio Bifurcation Front (KBF). This feature resembles the relationship between the eastern part of SPSTMW and the TF extension. This similarity between NPCMW and the eastern part of SPSTMW may explain why their temperature ranges are wider in the WOA 2001 climatology. Both mode waters may have separate types on either side of a front in a synoptic field, and this characteristic is smoothed out in the WOA 2001 climatology.

One conclusion from the comparison of SPSTMW, NPSTMW, and NPCMW using climatological data is that the range of CLT in STMWs is closely related to the flow pattern of the large-scale circulation. The West type and NPSTMW have almost uniform CLT and are located in the recirculation region of the subtropical gyre. The eastern part of SPSTMW and NPCMW may both have two types divided by temperature fronts. It is reasonable that STMW, located in the recirculation region, has almost uniform water properties because the streamlines are generally closed in the recirculation region.

The results of this study are merely the first step in comparing different STMWs. Further comparison will advance our knowledge of the features of STMWs. The detection and comparison of STMWs in the global ocean based on common criteria is under way and will be presented in an extension to the present study.

Acknowledgments. We thank Prof. Dean Roemmich for providing the latest version of HRX line data. The comments and English editing of Associate Prof. Frederick M. Bingham are also appreciated. We also express our sincere thanks to members of the Physical Oceanography Group at Tohoku University for fruitful discussions and to two anonymous reviewers for their constructive comments and English editing, which helped to improve this paper. This study was performed as a part of the 21st Century Center-Of-Excellence (COE) Program's Advanced Science and Technology Center for Dynamic Earth (E-ASTEC) at Tohoku University. Suga was supported in part by the Japan Society for the Promotion of Science (Grant-in-Aid for Science Research [B], 16340135).

REFERENCES

Akima, H., 1970: A new method of interpolation and smooth curve fitting based on local procedures. *J. Assoc. Comput. Mach.,* **17,** 589–603.

Bingham, F. M., 1992: Formation and spreading of Subtropical Mode Water in the North Pacific. *J. Geophys. Res.,* **97,** 11 177–11 189.

Boyer, T. P., C. Stephens, J. I. Antonov, M. E. Conkright, R. A. Locarnini, T. D. O'Brien, and H. E. Garcia, 2002: *Salinity*. Vol. 2, *World Ocean Atlas 2001,* NOAA Atlas NESDIS 50, CD-ROM.

Gilson, J., and D. Roemmich, 2002: Mean and temporal variability in Kuroshio geostrophic transport south of Taiwan (1993–2001). *J. Oceanogr.,* **58,** 183–195.

Gordon, A. L., J. R. E. Lutjeharms, and M. L. Grundlingh, 1987: Stratification and circulation at the Agulhas retroflection. *Deep-Sea Res.,* **34,** 565–599.

Hanawa, K., 1987: Interannual variations in the wintertime out-

crop area of Subtropical Mode Water in the North Pacific. *Atmos.–Ocean,* **25,** 358–374.

——, and I. Hoshino, 1988: Temperature structure and mixed layer in the Kuroshio region over the Izu Ridge. *J. Mar. Res.,* **46,** 683–700.

——, and J. Kamada, 2001: Variability of core layer temperature (CLT) of the North Pacific Subtropical Mode Water. *Geophys. Res. Lett.,* **28,** 2229–2232.

——, and L. D. Talley, 2001: Mode Waters. *Ocean Circulation and Climate: Observing and Modelling the Global Ocean*, G. Siedler et al., Eds., Academic Press, 373–386.

Maharaj, A. M., P. Cipolini, and N. J. Holbrook, 2005: Observed variability of the South Pacific westward sea level anomaly signal in the presence of bottom topography. *Geophys. Res. Lett.,* **32,** L04611, doi:10.1029/2004GL020966.

Masuzawa, J., 1969: Subtropical Mode Water. *Deep-Sea Res.,* **16,** 453–472.

Mulhearn, P. J., 1987: The Tasman Front: A study using satellite infrared imagery. *J. Phys. Oceanogr.,* **17,** 1148–1155.

Nakamura, H., 1996: A pycnostad on the bottom of the ventilated portion in the central subtropical North Pacific: Its distribution and formation. *J. Oceanogr.,* **52,** 172–188.

Oka, E., and T. Suga, 2003: Formation region of North Pacific Subtropical Mode Water in the late winter of 2003. *Geophys. Res. Lett.,* **30,** 2205, doi:10.1029/2003GL018581.

——, and ——, 2005: Differential formation and circulation of North Pacific Central Mode Water. *J. Phys. Oceanogr.,* **35,** 1997–2011.

Provost, C., C. Escoffier, K. Maamaatuaiahutapu, A. Kartavtseff, and V. Garcon, 1999: Subtropical Mode Waters in the South Atlantic Ocean. *J. Geophys. Res.,* **104,** 21 033–21 049.

Reynolds, R. W., N. A. Rayner, T. M. Smith, D. C. Stokes, and W. Wang, 2002: An improved in situ and satellite SST analysis for climate. *J. Climate,* **15,** 1609–1625.

Ridgway, K. R., and J. R. Dunn, 2003: Mesoscale structure of the mean East Australian Current System and its relationship with topography. *Prog. Oceanogr.,* **56,** 189–222.

Roemmich, D., and B. Cornuelle, 1990: Observing the fluctuations of gyre-scale ocean circulation: A study of the subtropical South Pacific. *J. Phys. Oceanogr.,* **20,** 1919–1934.

——, and ——, 1992: The Subtropical Mode Waters of the South Pacific Ocean. *J. Phys. Oceanogr.,* **22,** 1178–1187.

——, J. Gilson, J. Willis, P. Sutton, and K. Ridgway, 2005: Closing the time-varying mass and heat budgets for large ocean areas: The Tasman Box. *J. Climate,* **18,** 2330–2343.

Simmons, A., and J. Gibson, 2000: The ERA-40 project plan. ERA-40 Project Rep. Series 1, ECMWF, 63 pp.

Sprintall, J., D. Roemmich, B. Stanton, and R. Bailey, 1995: Regional climate variability and ocean heat transport in the southwest Pacific Ocean. *J. Geophys. Res.,* **100,** 15 865–15 871.

Stanton, B. R., 1979: The Tasman Front. *N. Z. J. Mar. Freshwater Res.,* **13,** 201–214.

Stephens, C., J. I. Antonov, T. P. Boyer, M. E. Conkright, R. A. Locarnini, T. D. O'Brien, and H. E. Garcia, 2002: *Temperature*. Vol. 1, *World Ocean Atlas 2001,* NOAA Atlas NESDIS 49, CD-ROM.

Suga, T., and K. Hanawa, 1990: The mixed-layer climatology in the northwestern part of the North Pacific subtropical gyre and the formation area of Subtropical Mode Water. *J. Mar. Res.,* **48,** 543–566.

——, and ——, 1995: The Subtropical Mode Water circulation in the North Pacific. *J. Phys. Oceanogr.,* **25,** 958–970.

——, Y. Takei, and K. Hanawa, 1997: Thermostad distribution in the North Pacific subtropical gyre: The Central Mode Water and the Subtropical Mode Water. *J. Phys. Oceanogr.,* **27,** 140–152.

Taneda, T., T. Suga, and K. Hanawa, 2000: Subtropical Mode Water variation in the northwestern part of the North Pacific subtropical gyre. *J. Geophys. Res.,* **105,** 19 591–19 598.

Tilburg, C. E., H. E. Hurlburt, J. J. O'Brien, and J. F. Shriver, 2001: The dynamics of the East Australian Current system: The Tasman Front, the East Auckland Current, and the East Cape Current. *J. Phys. Oceanogr.,* **31,** 2917–2943.

Wakata, Y., T. Setou, I. Kaneko, H. Uchida, and S. Imawaki, 2006: Interannual variability of the Kuroshio transport passing through the 137°E meridian in an OGCM related to the North Pacific windstress. *J. Oceanogr.,* **62,** 25–35.

Worthington, L. V., 1959: The 18°C water in the Sargasso Sea. *Deep-Sea Res.,* **5,** 297–305.

Yasuda, T., and Y. Kitamura, 2003: Long-term variability of North Pacific Subtropical Mode Water in response to spin-up of subtropical gyre. *J. Oceanogr.,* **59,** 279–290.